JOURNAL OF PROPULSION AND POWER
Vol 8, No. 2, March–April 1992

Structural and Aerodynamic Analysis of a Large-Scale Advanced Propeller Blade

O. Yamamoto* and R. August†
Sverdrup Technology, Inc., Brook Park, Ohio 44142

A finite element structure code and a finite difference Euler solver are combined to provide a more accurate analysis of a large-scale propfan. The NASTRAN finite element code is used to compute the blade deflection due to centrifugal and aerodynamic loads, and the NASPROP finite difference 3-D Euler code is employed to compute the steady-state aerodynamic load of the deflected blade. The effects of deflection on the aerodynamic and propeller performance characteristics are discussed. The local pressure profiles of deflected and undeflected blade models are compared with test data. The results show that improvements can be made by including proper blade deflection in the numerical model.

Introduction

THE advanced turboprop program (ATP) was initiated in the mid 1970s in order to develop a fuel-efficient propulsion system. The advanced turboprops, generally known as propfans, were designed to maintain high propulsive efficiency at high cruise speeds up to Mach 0.8.[1] To meet this requirement propfan blades employ large sweep and twist with thin airfoil sections to minimize compressibility losses.

In an earlier stage of the program, scaled models of several blade designs were tested in the wind tunnel. Over the past several years, as part of the large-scale propfan (LAP) program, 9-ft-diameter propellers have been tested in flight[2,3] as well as in the ONERA S1-MA wind tunnel at Modane, France.[4]

During development of the computational approach, earlier experiments provided a data base to validate various numerical codes. In recent years, numerical codes have been extensively used to simulate both inviscid[5–8] and viscous[9,10] as well as steady and unsteady flows[11,12] through the propfan. Over the years, numerical codes have evolved and have become sophisticated enough to be able to capture such complex flowfields as leading-edge and tip vortices and blade passage shock waves. Recently a series of Modane test cases[13] were simulated using two numerical schemes by Nallasamy et al.[14] The numerical predictions showed good agreement with the measured surface pressures. The report showed that the agreement of local pressure profiles varied between the inboard and outboard sections of the blade, and cited the uncertainty in the blade geometry with changes in the operating condition.

Numerical simulations in the past have not adequately accounted for the blade deflection associated with various operating conditions. Since propfans employ highly loaded thin blades, they experience more deflection than conventional propellers. In addition, large twist and sweep make the prediction of blade deflection more complex.

The propeller flow simulations are normally performed using a "hot shape," i.e., the design blade geometry of a propeller operating at a cruise condition. Previously, however, the same blade geometry has been used to compute propeller flowfields under off-design conditions, due to a lack of structural details. When a propfan is operated under a wide range of conditions, such as in Modane test cases where the Mach number ranges from 0.03 to 0.78, and the blade speed varies from 1200 rpm to 1800 rpm, the actual blade geometry under centrifugal and aerodynamic loads may be quite different from the design geometry.

In an attempt to correct for blade deflection, numerical simulations have adjusted the blade setting angle by a small amount depending upon the operating conditions. The amount of adjustment is usually estimated from previous experience, or by matching a computed performance parameter, typically the power coefficient, with the measured value. Furthermore the adjustment assumes that the entire blade is rigidly rotated uniformly, while actual blade deflection may be any combination of torsion and spanwise bending with amounts varying from hub to tip.

Srivastava et al.[15] included aeroelastic effects in their simulation of propfan flowfields, and reported that the power calculation varied up to 40% due to deflections.

The purpose of this paper is to study: 1) the nature of blade deformation under centrifugal and aerodynamic loads, and 2) the effects of blade deflection on the local pressure profiles and the overall performance characteristics.

Analysis

The overall structural-aerodynamic interaction approach is depicted in Fig. 1. Initially the blade speed (ω) and the nominal blade setting angle ($\beta_{3/4}$) are input to the NASTRAN code to generate the deflection under the centrifugal load (CL). Interface I is used to transfer the deflection data from NASTRAN onto the blade surface grid points used by the NASPROP aero code. The mesh generation code establishes the computational mesh around the deflected blade. With appropriate freestream Mach number and advance ratio, the NASPROP code proceeds to compute the propeller flowfield. Interface II extracts the surface pressures from the aerodynamic data, and the differential pressure (ΔP) is transferred onto the NASTRAN finite element nodes. After a new deflection under centrifugal and aerodynamic loads is computed, interface I establishes a new blade geometry, and the new computational mesh is generated for the second aerodynamic calculations. Structural-aerodynamic interaction is iterated until geometrical equilibrium is reached (loop 1). The variation of blade angle at the 75% radial location ($\Delta\beta_{3/4}$) is monitored for convergence.

When loop 1 is completed, the propeller performance characteristics are computed. In particular, predicted power coefficient (CP) is compared with the measured value. If the power comparison is not sufficiently close, the blade setting angle is adjusted, and the previous process is repeated until reason-

Presented as Paper 90-2401 at the AIAA/SAE/ASME/ASEE 26th Joint Propulsion Conference, Orlando, FL, July 16–18, 1990; received Aug. 9, 1990; revision received April 4, 1991; accepted for publication April 15, 1991.

*Sr. Research Engineer. Member AIAA.
†Director. Member AIAA.

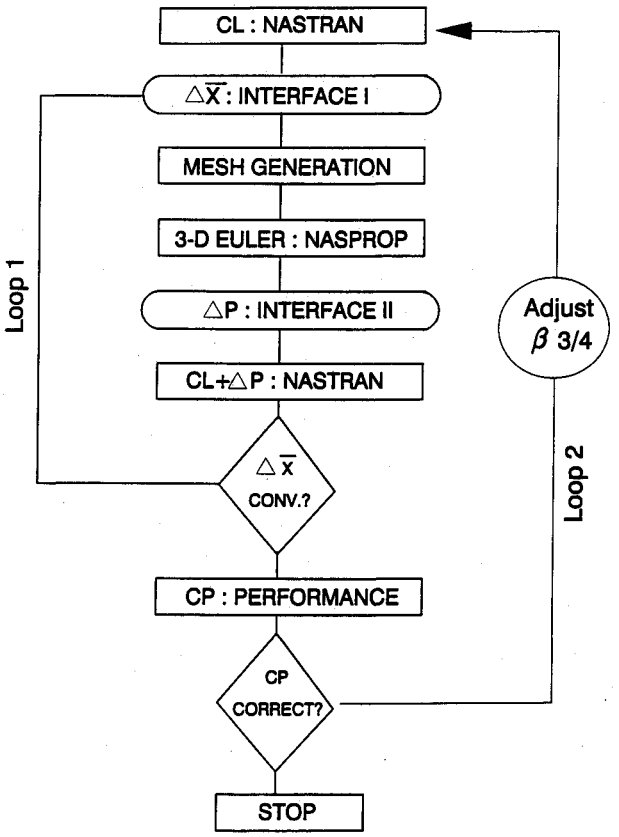

Fig. 1 Structure-aerodynamic integration.

able agreement in the power coefficient is obtained. This completes the loop 2 in Fig. 1.

Aerodynamic Analysis

The aerodynamic part of this work is performed by the NASPROP code. NASPROP is an implicit finite difference Euler solver originally developed by Bober et al.[16] to solve three-dimensional propeller flowfields, and was the first to provide detailed solutions of the advanced propeller flows. It employs the ADI scheme of Beam and Warming.[17] Since then the code has been rewritten incorporating improved boundary conditions, and has been vectorized for the CRAY computer.

The three-dimensional, inviscid flowfield about a propeller is governed by the Euler equations. The equations in conservative differential form are transformed from a cylindrical coordinate system to a time-dependent, body-fitted curvilinear reference frame, with the equations cast in nondimensional form.

First-order-accurate implicit Euler time differencing is employed, and the spatial derivatives are replaced by central differences with appropriate one-sided differences at the boundaries. The resulting implicit operators involve inversions of a block tridiagonal system. The system can be reduced to scalar tridiagonal matrices by applying a diagonalization technique[18] to the flux Jacobian matrices. Constant coefficient, second-order implicit and fourth-order explicit dissipation terms are added for stability considerations. A periodic tridiagonal matrix inversion is employed in the circumferential direction except on the blade surfaces. Further details of the solution procedure and the implementation of the boundary conditions can be found in Refs. 5 and 6.

In this paper, the steady-state propeller flowfield with the propeller axis at zero angle of attack is computed. Hence, only one blade passage needs to be considered in the computational domain. The flowfield is assumed to be periodic in the blade-to-blade direction. A typical computational mesh is shown in Fig. 2. A total of 101 × 33 × 45 grid points are used for the mesh, and 41 × 21 grid points are distributed on each surface of the blade.

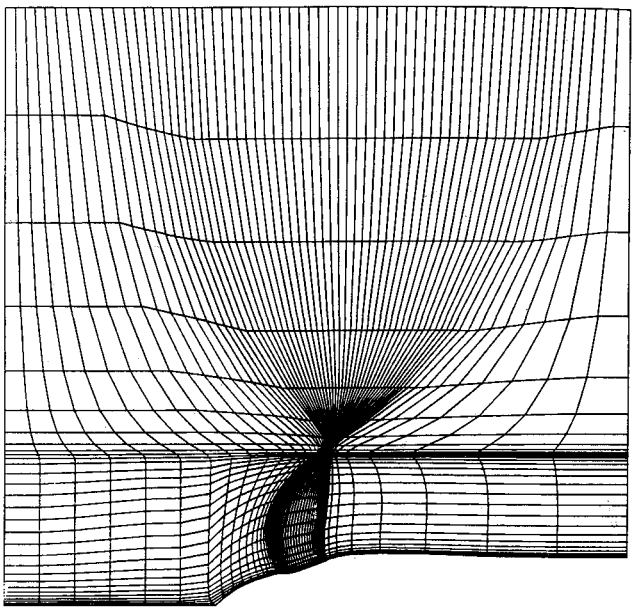

Fig. 2 NASPROP grid.

Structural Analysis

The unique design features incorporated into advanced propfans such as the SR7L require the use of finite element codes for the blade's structural analysis. In addition to the design, the use of composite materials also requires special attention in the structural modeling. These thin, twisted, and highly swept blades, manufactured with nonisotropic materials experience large, nonlinear deflections due to blade flexibility, and combined centrifugal and aerodynamic loads.

MSC/NASTRAN was used to calculate the SR7L steady-state deflections because it has the capability to perform geometric nonlinear analysis as well as the capability to update the displacement-dependent centrifugal forces. MSC/NASTRAN solution 64 was used for the geometric nonlinear analysis. This solver uses a modified Newton-Raphson algorithm, along with load updating, to simulate the correct displacement versus load relationship.

The algorithm iterations are controlled through "subcases," with a minimum of two being required. The first subcase computes the initial, linear deflected shape. Subsequent subcases, or iterations, then use the previously deflected shape to compute the differential stiffness matrix along with the new set of displacements. For this analysis, 14 subcases were used to achieve a converged, displacement vector. In addition, NASTRAN Direct Matrix Abstraction Program (DMAP) procedures are included in the analysis to account for centrifugal softening due to the centrifugal forces acting in the same direction as the displacement. A detailed explanation of the above procedures is given in Ref. 19.

The NASTRAN finite element model used in this study is based on the final SR7L design.[20] The blade geometry and airfoil data were obtained from the engineering design drawings. The composite material properties were calculated by a micromechanics approach using available fiber and matrix properties from actual testing of the material. The SR7L blade has an aluminum spar, fiberglass shell with foam fill, and nickel alloy sheath. All these materials were combined using the Composite Blade Structural Analysis (COBSTRAN) program to produce equivalent, monolithic shell elements.[21]

The SR7L finite element model is shown in Fig. 3a. It has 261 nodes. The blade is modeled using 449 triangular shell elements (NASTRAN element CTRIA3). Five bar elements (NASTRAN element CBAR) are used to model the blade shank. Multipoint constraint cards that couple the displace-

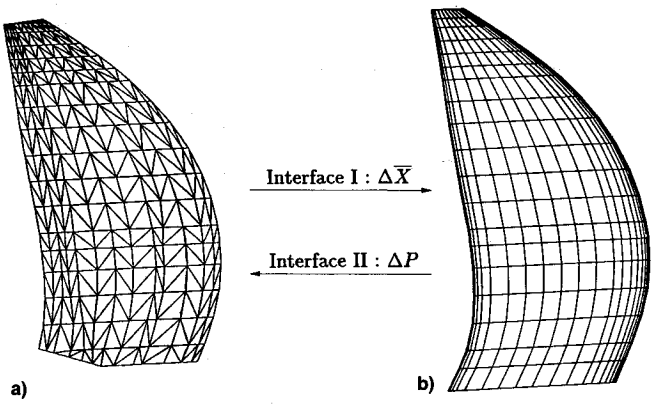

Fig. 3 Chord planes: a) NASTRAN; b) NASPROP.

ment of prescribed grid points are used to define the blade–shank interface. The blades are structurally decoupled from one another by assuming a rigid hub; thus necessitating that only one blade be modeled. To accurately simulate the shank–hub compliance, the blade shank constraints were modeled by using spring elements (NASTRAN element CELAS) attached to the base of the shank. A total of 4 DOF for the shank base were allowed; translation along the pitch change axis, bending rotations in and out of the plane of rotation, and rotation about the blade's pitch change axis.

Verification of the finite element model is done by comparing calculated and experimental results. This finite element model was originally developed for aeroelastic studies of flutter and forced response. Consequently, the model's validity is checked by quantitatively comparing natural frequencies and qualitatively comparing mode shapes over a range of speeds. The details of this comparison are given in Ref. 22. The good agreement of the dynamic properties implies the blade's stiffness matrix is being properly formulated. Therefore, the calculated steady deflections are reasonably accurate.

Interfaces

While the structural deformations are computed at the finite element model grid points, aerodynamic forces are computed on the blade surface grid points. To make the exchange of data between the structural and aerodynamic analyses possible, the surface grid points used in the aerodynamic calculations are projected onto a plane identical to the structural model. The plane is constructed by connecting each chord line of airfoil sections that define the blade geometry. The aero chord plane is shown in Fig. 3b.

Differences in the number and the distribution of grid points necessitate an interpolation of data between the two models. Two-dimensional cubic spline is used for the data interpolation.

In interface I, the nodal displacements from the structural model are interpolated onto the grid points of the aero chord plane. Then the displacements are vectorially added to the corresponding surface grid coordinates. The procedure is reversed in interface II. The pressure from the NASPROP calculations are first projected onto the aero chord plane, then the differential pressures (ΔP) are computed. ΔP is transferred to the structural model using interpolation. For the structural analysis, pressure loads at the grid points are generated and appended to the NASTRAN input deck.

Results and Discussion

The approach discussed above is applied to the two-bladed, 9-ft-diameter, SR7L propfan. Computations are performed on a CRAY-XMP computer for NASTRAN calculations, and CRAY-XMP and -YMP computers for NASPROP calculations. Two interfaces between NASTRAN and NASPROP are performed on a AMDAHL 5860 computer.

Since the displacement at each grid point is added vectorially to the blade surface coordinates, the deflection can result in three basic modes of deformation: 1) twisting, 2) spanwise bending, and 3) change in the section camber. The effects of camber are expected to be small, and thus they are not discussed in this report.

First, the deflection pattern under centrifugal load (CL) alone is shown in Figs. 4 and 5. The change in local blade angle ($\Delta\beta$), as a measure of twisting, and the variation of local face alignment distance, as a measure of spanwise bending, are shown in Figs. 6 and 7. The blade is operated at 1842 rpm and the blade angle at the $\frac{3}{4}$ radius is set to 54.5 deg. The maximum blade twist is observed to be -2.5 deg at the tip,

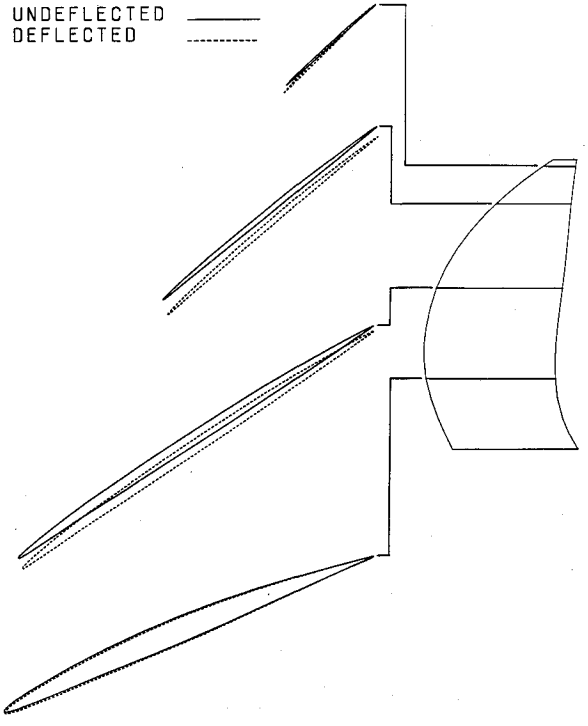

Fig. 4 Chordwise deflection.

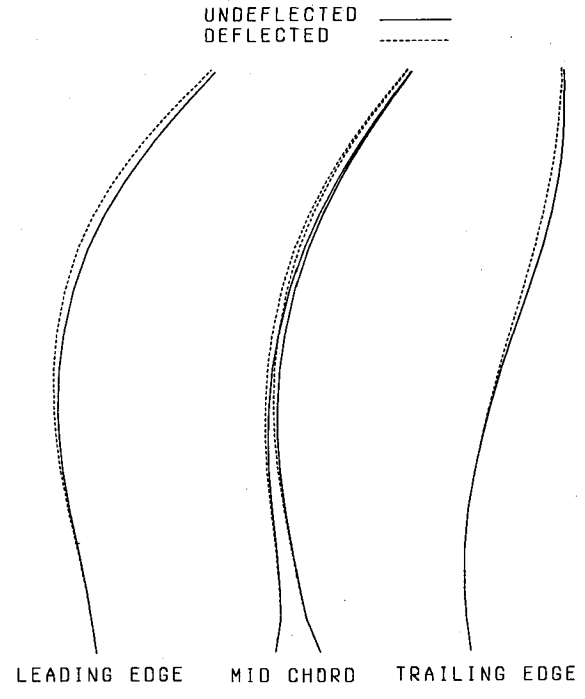

Fig. 5 Spanwise deflection.

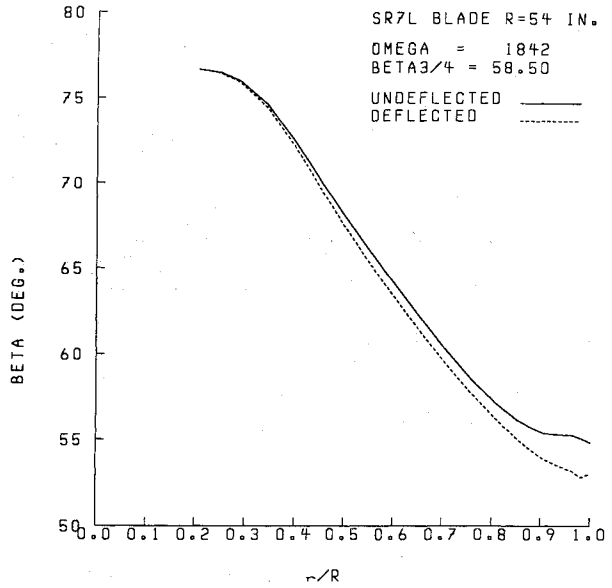

Fig. 6 Variation of local blade angle.

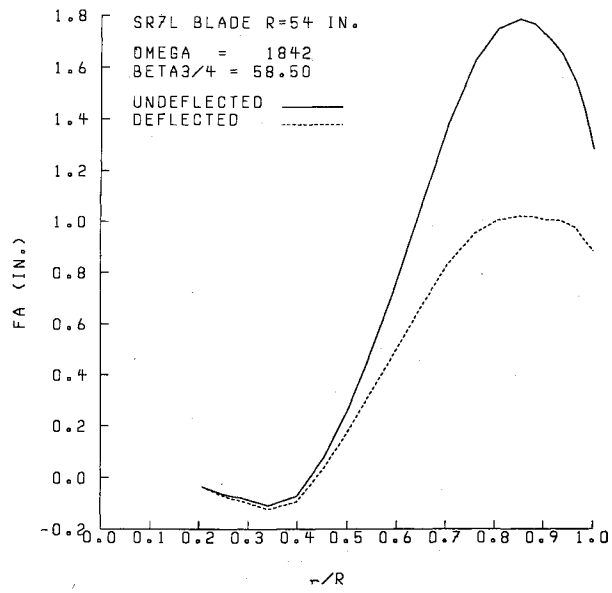

Fig. 7 Variation of face alignment distance.

and the maximum bending is approximately 0.8 in. at 85% radius. The centrifugal load tends to untwist the blade, heavily near the tip, and tends to straighten the blade.

During the LAP test conducted in Modane,[4] the two-bladed propfan was operated at a wide range of conditions. In order to assess the range of deflections, the parametric effects of blade speed and blade setting angle on blade twist are shown in Fig. 8. For convenience the change in blade twist at the ¾ radius is computed as the blade speed and the blade angle are varied. The figure shows that under a practical range of operating conditions, the blade setting angle has much less effect on the blade deflection than the blade speed, especially at low speeds. The range of twist is shown to be −0.3 deg at 1200 rpm to −0.8 deg at 1842 rpm. The corresponding range of maximum bending is computed to be 0.6 to 0.8 in. From previous experience, the amount of blade twist indicated here is expected to produce significant change in the performance calculations.

Two Modane test cases are chosen to demonstrate the structural-aerodynamic analysis procedure. Modane test 7 is a high-power loading and low-blade-speed case. The measured power coefficient and blade speed are 0.642 and 1192 rpm, respec-

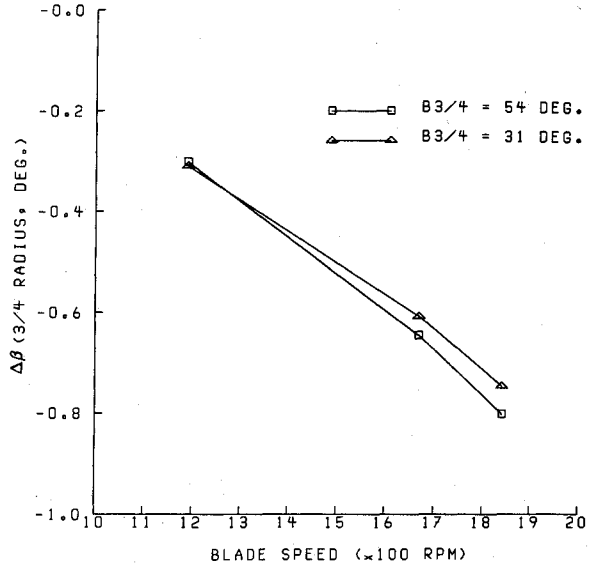

Fig. 8 Effects of blade speed and blade angle.

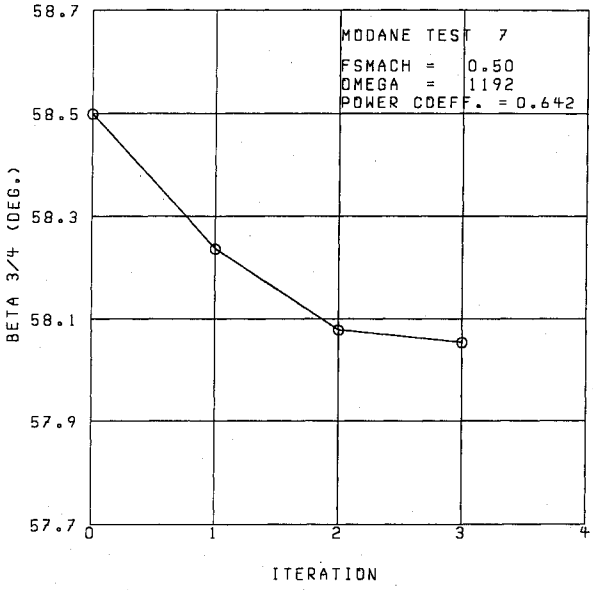

a) Modane test 7, $M = 0.5$.

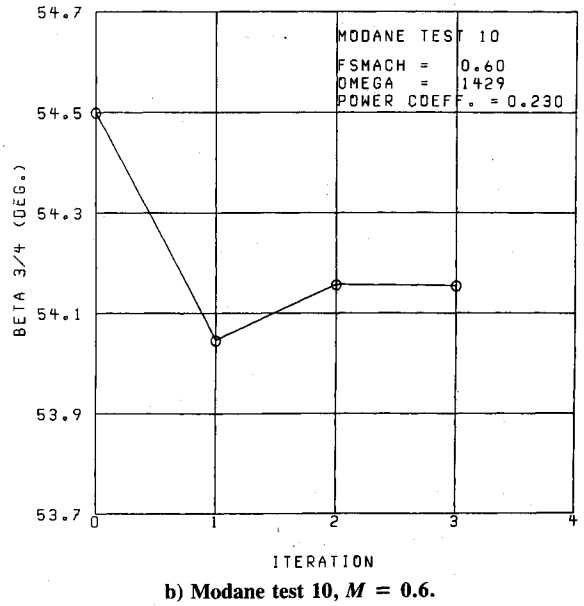

b) Modane test 10, $M = 0.6$.

Fig. 9 Variation of blade angle with structure-aerodynamic interaction.

tively. Modane test 10, on the contrary is a low-power (CP = 0.23) and higher blade speed (1429 rpm) case. The Mach number and the blade angle are 0.5 and 58.5 deg for test 7, and 0.6 and 54.5 deg for test 10.

Figures 9a and 9b show the variation of blade angle at $\frac{3}{4}$ radial location with structural-aerodynamic iteration. ITER 1 denotes the deflection due to centrifugal load alone, ITER 2 and 3 for the deflection with subsequent aero load added. Figs. 10a and 10b show the corresponding variations of computed power coefficient. Two iterations of aero load (ITER 3) calculations are shown to be sufficient for convergence. Loop 2 is iterated twice to meet the power comparison.

In each test case, the centrifugal load produces most of the total deflection, with the blade deflecting into the plane of rotation. As an assessment of power change, Figs. 9b and 10b show that a 0.45-deg decrease in the blade angle results in 11% reduction in the power coefficient. While the centrifugal load always results in reduced blade angle, the changes due to aero loads are not uniform. The first application of aero load results in increased blade angle in test 10, and an opposite trend is shown in test 7.

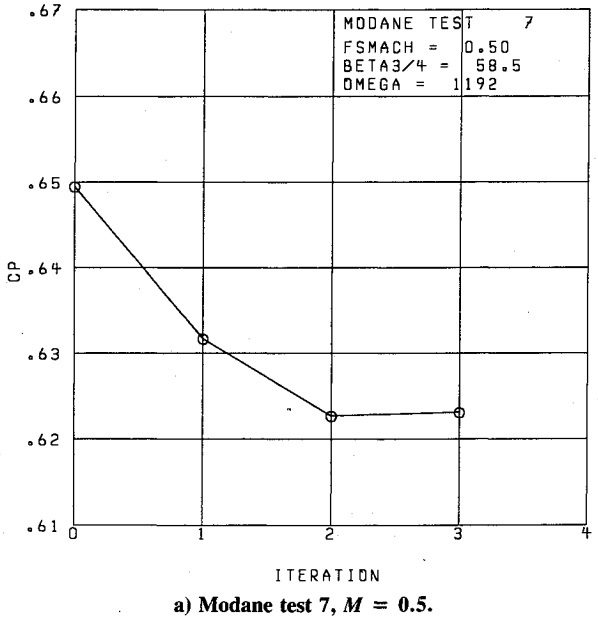

a) Modane test 7, $M = 0.5$.

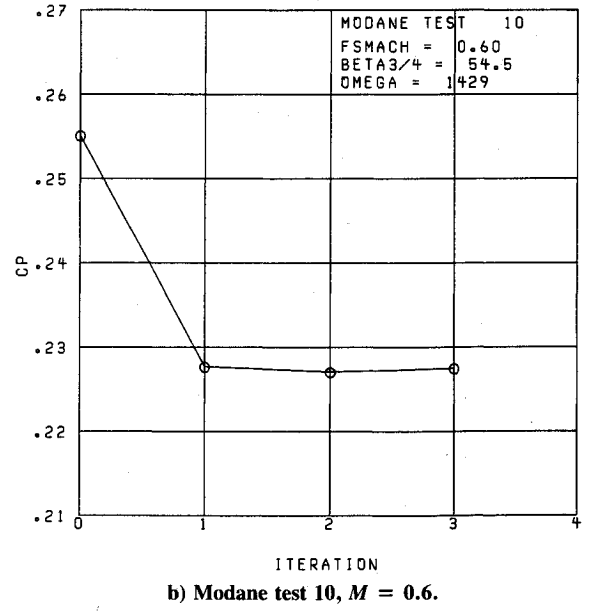

b) Modane test 10, $M = 0.6$.

Fig. 10 Variation of power coefficient with structure-aerodynamic interaction.

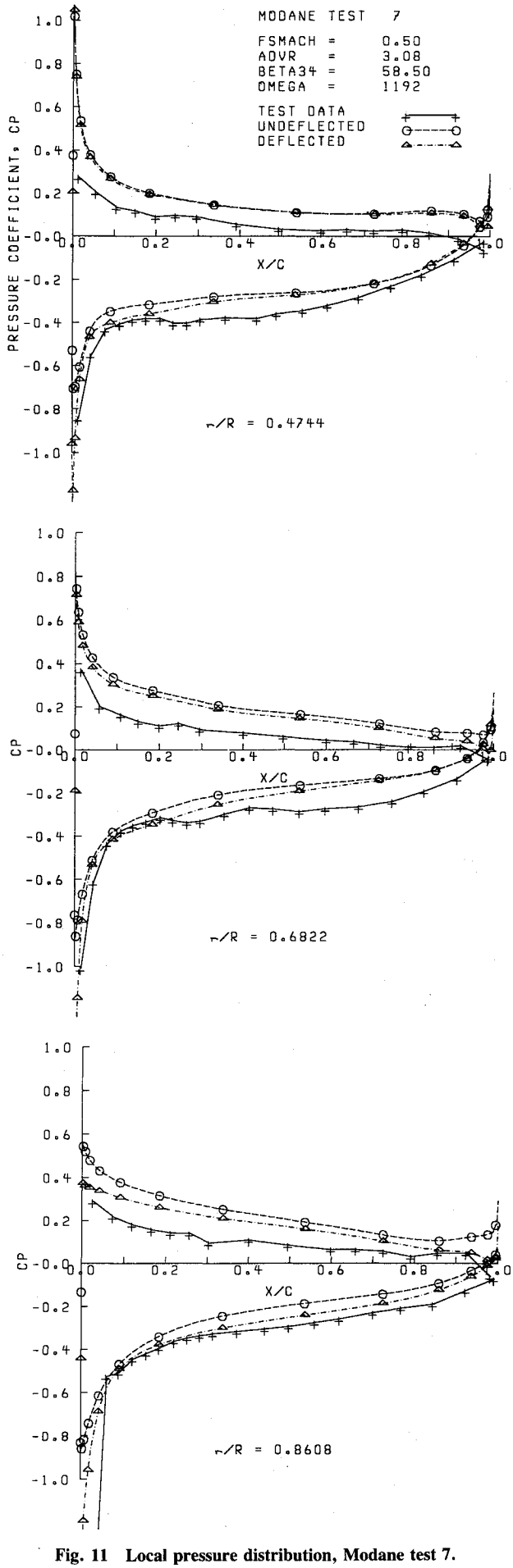

Fig. 11 Local pressure distribution, Modane test 7.

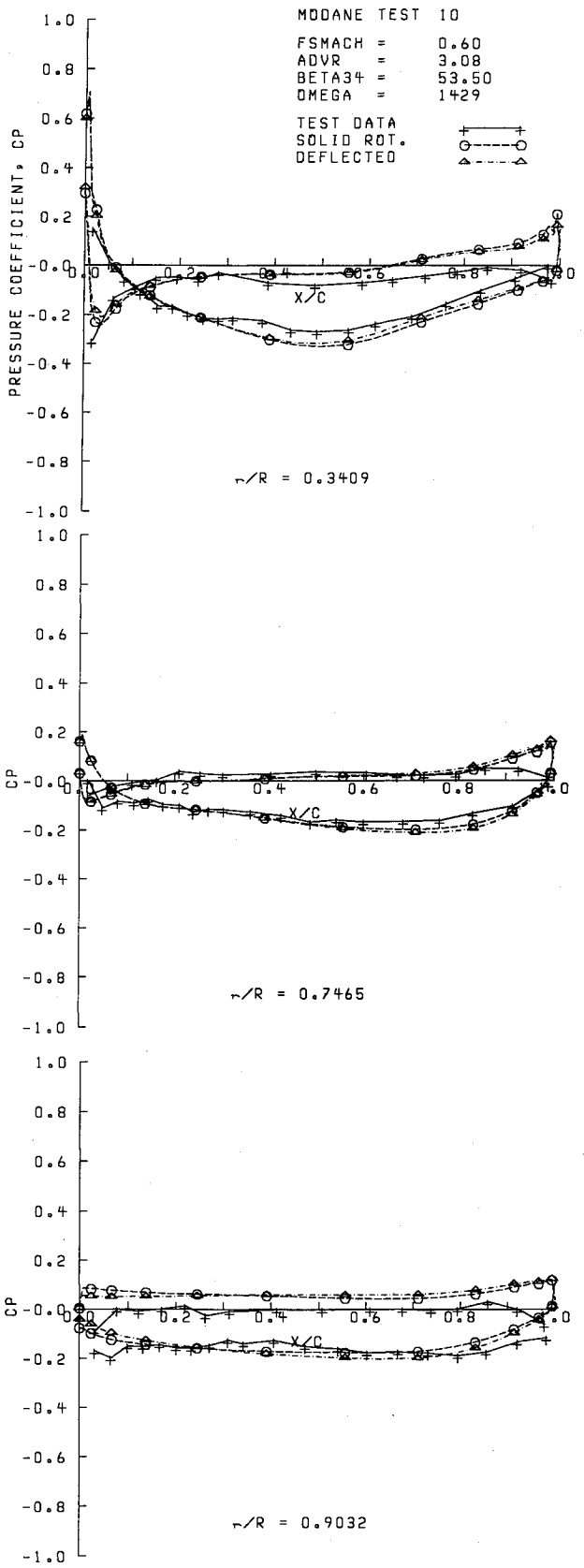

Fig. 12 Local pressure distribution, Modane test 10.

In order to understand the effect of aerodynamic load, one must study the local pressure distribution on the blade. The pressure profiles of tests 7 and 10 are shown in Figs. 11 and 12. The test data are shown as a reference. The comparisons between the test data and the numerical prediction are similar to the results of Nallasamy et al.[14] In Fig. 11, a comparison between the undeflected and the deflected (CL + aero) blades is made. The difference between the two pressure profiles is small on the inboard section as expected from the assumption that the deflection is negligibly small at the hub. The difference grows as the radial distance increases. Although the discrepancy between the test data and the prediction on the pressure side is large, favorable correction is indicated by the deflected model. On the outboard section, the pressure profile improves significantly near the trailing edge where the structure is known to be flexible and susceptible to deflection.

A comparison between a solid body rotation of the blade and the fully deflected blade is made in Fig. 12. The solid body rotation of blade has been used in the past to simulate the deflected blade. The solid body rotation is accomplished by rotating the entire blade about the pitch change axis uniformly from hub to tip. The amount of adjustment is determined by matching the computed power coefficient with the measured value.

The difference between the two predictions remains small throughout the blade, indicating that the solid body rotation provides a reasonable correction for the undeflected blade. However, a shift in the pressure loading is observed from the inboard section to outboard. On the outboard section of the blade, the solid rotation results in higher pressure loading in the forward section and less toward the aft section. This is because the rigidly rotated blade has a higher local blade angle than the fully deflected blade which has the untwisted blade tip due to centrifugal load. The opposite trend is observed on the inboard section of the blade. The deficiency of solid body rotation is that it is difficult to predict consistent pressure loading from hub to tip.

Comparing pressure profiles of the two test cases, test 10 is shown to have more pressure loading in the aft section than in the forward section. In contrast, pressure loading is concentrated in the forward section in test 7. This difference in the aerodynamic loading seems to result in the distinctly different deflection trends shown in Figs. 9a and 9b. When the forward region is highly loaded, the aerodynamic effect tends to untwist the blade while high tail loading results in increased local blade angle. Unlike the centrifugal deflection, the effect of aero load cannot be determined a priori until the local pressure distribution is analyzed.

Conclusions

Blade deflection can be described in terms of blade twist, spanwise bending, and change in section camber. For steady-state loading, effects of spanwise bending on the aerodynamic characteristics are considered to be small compared to twist and camber effects. However, when unsteady loading or the propeller at an angle of attack is considered, spanwise bending may become an important factor. The position of the blade section relative to the freestream is critical in those flows.

It is shown that the centrifugal load produces most of the total deflection. A comparable amount of blade twist can be produced by aero load when the blade speed is low and the power loading is high. Blade twist due to centrifugal load depends mostly on the blade speed, and less on the blade angle. While the centrifugal load tends to untwist the blade, no simple relation holds for the aerodynamic load. Blade twist due to aero load depends on the local pressure distribution. Loading in the forward section tends to untwist, and tail loading results in twist of blade section.

The fully deflected model showed better agreement with the test data than the undeflected model. Significant improvement was observed on the outboard aft section where the blade is structurally flexible for deflection. Solid rotation of the blade can provide some correction for the deflection; however, consistent agreement with measured pressure data is difficult to maintain throughout the blade.

The analysis technique described in this paper can readily be used in conjunction with a Navier-Stokes code for further refinement of numerical predictions. Also the analysis can be adapted to compute deflection under unsteady aerodynamic

loads. Although it will be computationally expensive to evaluate the deflection at each time step, a scheme can be devised to reduce the cost by computing the deflection at specified intervals.

References

[1]Whitlow, J. B., Jr., and Sievers, G. K., "Fuel Savings Potential of the NASA ATP," NASA TM 83736, 1984.

[2]Poland, D. T., Bartel, H. W., and Brown, R. C., "PTA Flight Test Overview," AIAA Paper 88-2803, July 1988.

[3]Poland, D. I., Bartel, H. W., Reddy, N. N., Swift, G., and Withers, C. C. "Propfan Test Assessment (PTA) Flight Test Report," NASA CR-182278, 1989.

[4]Campbell, W. A., Wainauski, H. S., and Bushnell, P. R., "A Report on High Speed Wind Tunnel Tests of the Large Scale Advanced Propfan," AIAA Paper 88-28, 1988.

[5]Barton, J. M., Yamamoto, O., and Bober, L. J., "Euler Analysis of Transonic Propeller Flows," *Journal of Propulsion and Power*, Vol. 3, No. 3, 1987, pp. 277–282.

[6]Yamamoto, O., Barton, J. M., and Bober, L. J., "Improved Euler Analysis of Advanced Turboprop Propeller Flows," AIAA Paper 86-1521, June 1986.

[7]Nallasamy, M., Clark, B. J., and Groeneweg, J. F., "Euler Analysis of the Three-Dimensional Flow Field of a High Speed Propeller: Boundary Condition Effects," *Journal of Turbomachinery*, Vol. 109, No. 3, 1987, pp. 332–339.

[8]Saito, S., Kobayashi, H., Wada, Y., and Matsuo, Y., "Numerical Approach of Advanced Turboprop with Three-Dimensional Euler Equations," SAE Paper 87-2448, 1987.

[9]Matsuo, Y., Saito, S., Arakawa, C., and Kobayashi, H., "Navier-Stokes Computations for Flowfield of an Advanced Turboprop," AIAA Paper 88-3094, 1988.

[10]Saito, S., and Kobayashi, H., "Navier-Stokes Simulations Around a Propfan Using Higher-Order Upwind Schemes," AIAA Paper 89-2699, July 1989.

[11]Whitfield, D. L., Swafford, T. W., Janus, R.A., Mulac, R. A., and Belk, D. M., "Three-Dimensional Unsteady Euler Solutions for Propfan and Counter Rotating Propfans in Transonic Flow," AIAA Paper 87-1197, 1987.

[12]Nallasamy, M., and Groeneweg, J. F., "Unsteady Euler Analysis of the Flow Field of a Propfan at an Angle of Attack," AIAA Paper 90-0339, Jan. 1990.

[13]Bushnell, F., "Measurement of the Steady Surface Pressure Distribution on a Single Rotation Large Scale Advanced Propfan Blade at Mach Numbers from 0.03 to 0.78," NASA CR-182124, 1988.

[14]Nallasamy, M., Yamamoto, O., Warsi, S., and Bober, L. J., "Large Scale Advanced Propeller Blade Pressure Distributions: Prediction and Data," NASA TM 102316, 1989.

[15]Srivastava, R., Sankar, N. L., Reddy, T. S. R., and Huff, D. L., "Application of an Efficient Hybrid Scheme for Aeroelastic Analysis of Advanced Propellers," AIAA Paper 90-0028, Jan. 1990.

[16]Bober, L. J., Chaussee, D. S., and Kutler, P., "Prediction of High Speed Propeller Flow Field Using a Three-Dimensional Euler Analysis," NASA TM 83065, 1983.

[17]Beam, M., and Warming, R. F., "An Implicit Finite-Difference Algorithm for Hyperbolic Systems in Conservation Law Form," *Journal of Computational Physics*, Vol. 22, No. 1, 1976, pp. 87–110.

[18]Pulliam, T. H., and Chaussee, D. S., "A Diagonal Form of an Implicit Approximate Factorization Algorithm," *Journal of Computational Physics*, Vol. 39, No. 2, 1981, pp. 347–363.

[19]Lawrence, C., et al., "A NASTRAN Primer for the Analysis of Rotating Flexible Blades," NASA TM 89861, May 1987.

[20]Sullivan, W. E., Turnber, J. E., and Violette, J. A., "Large-Scale Advanced Propfan (LAP) Blade Design," NASA CR 174790.

[21]Aiello, R. A., and Chi, S., "Advanced Composite Turboprops: Modeling, Structural and Dynamic Analysis," ASME Paper 87-GT-78, 1987.

[22]August, R., and Kaza, K. R. V., "Vibration, Performance, Flutter and Forced Response Characteristics of a Large Scale Propfan and Its Aeroelastic Model," NASA TM 101322, 1988.